

Single-particle excitations and phonon softening in the one-dimensional spinless Holstein model

S. Sykora^a, A. Hubsch^{a,b}, K. W. Becker^a, G. Wellein^c, and H. Fehske^d

^aInstitut für Theoretische Physik, Technische Universität Dresden, D-01062 Dresden, Germany

^bDepartment of Physics, University of California, Davis, CA 95616, USA

^cRegionales Rechenzentrum Erlangen, Universität Erlangen-Nürnberg, Germany and

^dInstitut für Physik, Ernst-Moritz-Armdt Universität Greifswald, D-17487 Greifswald, Germany

(dated: April 14, 2024)

We investigate the influence of the electron-phonon coupling in the one-dimensional spinless Holstein model at half-filling using both a recently developed projector-based renormalization method (PRM) and an refined exact diagonalization technique in combination with the kernel polynomial method. At finite phonon frequencies the system shows a metal-insulator transition accompanied by the appearance of a Peierls distorted state at a finite critical electron-phonon coupling. We analyze the opening of a gap in terms of the (inverse) photoemission spectral functions which are evaluated in both approaches. Moreover, the PRM approach reveals the softening of a phonon at the Brillouin-zone boundary which can be understood as precursor effect of the gap formation.

PACS numbers: 71.10.Fd, 71.30.+h

I. INTRODUCTION

Despite the many years of study of the electron-phonon interaction in metallic systems, there remain fundamental problems that yet have to be resolved. Especially systems which suffer strong electron-phonon coupling in conjunction with strong electron-electron interaction are in the center of present interest. Examples are cuprate high-temperature superconductors^{1,2}, colossal magnetoresistive manganites³, or metallic alkaline-doped C₆₀-based compounds. Furthermore, in a wide range of quasi-one-dimensional materials, such as MX chains, conjugated polymers or organic charge transfer complexes⁴, the itinerancy of the electrons strongly competes with the electron-phonon coupling which tends to establish e.g. charge-density-wave structures. Then, in particular at half-filling, Peierls insulating phases may be energetically favored over the metallic state. Many interesting questions arise not only with a view to the associated metal to insulator transition but also concerning the form of the single-particle excitation spectra well below and above the transition. At present, there is a clear need of reliable theoretical methods to tackle these problems in terms of microscopic models.

In this paper we study as the perhaps simplest realization of a strongly coupled electron-phonon system, the so-called spinless Holstein model, describing the local interaction between dispersionless longitudinal optical phonons and the density of the electrons at a given lattice site $n_i = c_i^\dagger c_i$:

$$H = \sum_{i,j} t_{ij} (c_i^\dagger c_j + \text{h.c.}) + \sum_i !_0 \left(b_i^\dagger b_i + g \left(b_i^\dagger + b_i \right) n_i \right) \quad (1)$$

Here, c_i^\dagger (b_i^\dagger) denote fermionic (bosonic) creation operators of electrons (phonons), i is the Wannier site index. The electron-phonon coupling constant and frequency of the Einstein mode is given by g and $!_0$, respectively. Of physical concern for most applications are relatively small values of the adiabaticity ratio $\gamma = !_0/t \ll 1$, even though the anti-adiabatic limit $\gamma \gg 1$ is also a useful point of reference for an overall understanding of the physics of the Holstein model.

It is well-known that the one-dimensional Holstein model of spinless fermions at half-filling has a quantum phase transition from a Luttinger liquid (metallic phase) to an insulating phase with charge-density wave long-range order^{5,6,7}. In the past, a large number of different analytical and numerical methods have been applied to the Holstein model, in particular to determine the phase boundary between metallic and insulating behavior for the half-filled band case. Much of the work is restricted to the one-dimensional case. Mainly ground state properties were investigated by means of strong-coupling expansions⁵, variational⁸ and renormalization group^{6,9} approaches, as well as world-line quantum Monte Carlo⁵ and Green's-function Monte Carlo¹⁰ simulations. More recently, exact diagonalization¹¹ (ED) and density matrix renormalization group^{7,12,13,14} techniques were applied. The metal-insulator transition is accompanied by the appearance of a gap in the electronic spectrum which, however, can best be observed in the k -dependent one-particle spectral functions. In a recent dynamical mean field treatment¹⁵ in conjunction with a numerical renormalization group approach it was suggested that the opening of the electronic gap is accompanied by the appearance of a low-energy phonon peak in the total phononic spectral function. In fact, we shall show in this paper that the phonon modes at the Brillouin-zone boundary become soft. This can be understood as a precursor effect of a lattice

instability leading to a Peierls state for electron-phonon coupling strength g larger than some finite critical value g_c . Moreover, we shall evaluate electronic one-particle spectral functions which should show the opening of the gap at the quantum phase transition. The evaluation of Luttinger parameters is beyond the scope of interest of this paper.

One of the main aims of the paper is to show that a newly developed projector-based renormalization method (PRM) for many-particle Hamiltonians¹⁶ can be applied to the spinless Holstein model, though an extension to the case with spin would also be possible. In principle this method is applicable to infinitely large systems, to the whole parameter regime of the electron-phonon coupling $g \neq 0$, to any filling, and to any spatial dimension. In the present paper we restrict ourselves to the case of one dimension and to half-filling in order to study the transition from the metallic to the insulating phase. It will turn out the Peierls instability associated with the metal-insulator transition can very well be described in the present formalism. Since the application of the PRM, however, is accompanied by some approximations, the reliability of the technique will be tested by comparing its results with unbiased data from exact diagonalization (ED). In particular, the k -dependent one-particle spectral functions from (inverse) photoemission will be analyzed within both approaches. As is seen, the formation of a charge gap at some critical value g_c of the electron-phonon coupling is related to the softening of phonon modes at the Brillouin-zone boundary, at least in the adiabatic regime. From the ED data we get additional valuable insights into the behavior of the wave-vector resolved spectral function. Moreover, a detailed characterization of the ground state, e.g. by the phonon distribution is possible. We note that the present approach is not restricted to large dimensions as is the case of a recent DMFT approach¹⁵.

The paper is organized as follows. In Sect. II we outline the PRM approach¹⁶. The renormalization equations for the model parameters are derived non-perturbatively and general expressions for the one-particle spectral functions are discussed. In Sect. III we discuss our exact diagonalization technique for the calculation of single-particle spectral functions of coupled electron-phonon systems. Sect. IV presents the findings obtained within both approaches for the (I)PE spectra and phonon renormalization, in particular with respect to the metal to Peierls insulator transition in the 1D Holstein model. The main results will be summarized in Sect. V.

II. RENORMALIZATION OF THE HOLSTEIN MODEL

A. Projector-based renormalization method

The PRM¹⁶ starts from a decomposition of a given many-particle Hamiltonian H into an unperturbed part H_0 and a perturbation H_1

$$H = H_0 + H_1; \quad (2)$$

where we assume that the eigenvalue problem of H_0 is solved

$$H_0 |n^{(0)}\rangle = E_n^{(0)} |n^{(0)}\rangle; \quad (3)$$

The decomposition of H into H_0 and H_1 should be done in such a way that H_1 contains no part which commutes with H_0 . Thus, H_1 gives rise to transitions between eigenstates of H_0 with different eigenenergies. The presence of H_1 usually prevents the exact solution of the eigenvalue problem of the full Hamiltonian. Let us define a projection operator P by

$$P A = \sum_{m,n} |n^{(0)}\rangle \langle m^{(0)}| A |m^{(0)}\rangle \langle n^{(0)}| \quad (E_n^{(0)} - E_m^{(0)})^{-1} \quad (4)$$

P is a super-operator which acts on ordinary operators A of the unitary space. It projects on those parts of A which are formed by transition operators $|n^{(0)}\rangle \langle m^{(0)}|$ with energy differences $E_n^{(0)} - E_m^{(0)}$ less than a given cutoff ϵ , where ϵ is smaller than the cutoff of the original model. Note that in Eq. (4) neither $|n^{(0)}\rangle$ nor $|m^{(0)}\rangle$ have to be low-energy eigenstates of H_0 . However, their energy difference has to be restricted to values $< \epsilon$. Furthermore we define the projector

$$Q = 1 - P \quad (5)$$

on the high-energy transitions larger than the cutoff ϵ , ($Q P = 0$).

Now we want to transform the initial Hamiltonian H of Eq. (1) into an effective Hamiltonian H_{eff} which has no matrix elements belonging to transitions larger than ϵ . This will be achieved by a unitary transformation

$$H_{\text{eff}} = e^X H e^{-X}; \quad (6)$$

where the generator X of the transformation has to be anti-Hermitian, i.e. $X^\dagger = -X$. Note that the effective Hamiltonian H has the same eigenspectrum as the original Hamiltonian H . The generator X has to be chosen such that H has no matrix elements between states belonging to transitions larger than Δ . Hence the condition

$$Q H = 0 \quad (7)$$

has to be fulfilled. Eq. (7) will be used below to specify X .

Instead of eliminating all high-energy excitations in one step a sequence of stepwise transformations will be used in the following. Thus, in an infinitesimal formulation, the projector-based renormalization approach yields renormalization equations for the parameters of the Hamiltonian as function of the cutoff. In that aspect the present approach resembles Wegner's flow equation method¹⁷ and the similarity transformation introduced by Glatzek and Wilson¹⁸. To find the renormalization equations we proceed as follows. We start from the renormalized Hamiltonian

$$H = H_{0;'} + H_{1;'}; \quad (8)$$

where in H all excitations with energy differences larger than Δ have been eliminated. Next we further integrate out all excitations inside an energy shell between Δ and a smaller cutoff Δ' ($\Delta' < \Delta$) where $\Delta' > 0$. The new Hamiltonian $H(\Delta')$ is given by

$$H(\Delta') = e^X H e^{-X}; \quad (9)$$

where $X_{\Delta'}$ is the generator for the transformation from Δ to Δ' . Similar to (7) it has to fulfill the condition

$$Q(\Delta') H(\Delta') = 0: \quad (10)$$

Note that there are two strategies to exploit Eq. (10) in order to determine the generator $X_{\Delta'}$ of the unitary transformation (9). The most straightforward route is to analyze Eqs. (9) and (10) in perturbation theory as it was done in Refs. 16 and 19. Here, we want to perform the renormalization step from Δ to Δ' in a non-perturbative way which recently has been applied to the periodic Anderson model by two of the authors²⁰.

Eqs. (9) and (10) can be used to derive difference equations for the dependence of the parameters of the Hamiltonian. They will be called renormalization equations. The solution depends on the initial values of the parameters of the Hamiltonian and fixes the renormalized Hamiltonian H in the limit $\Delta \rightarrow 0$. Note that the renormalized Hamiltonian only consists of an renormalized unperturbed part $H_{0;(\Delta \rightarrow 0)}$. The interaction $H_{1;(\Delta \rightarrow 0)}$ completely vanishes since it was used up in the renormalization procedure.

B. Application to the Holstein model

Let us start by formally writing down the effective Hamiltonian $H = e^X H e^{-X}$ for the spinless Holstein model after all excitations with energy differences larger than Δ have been eliminated,

$$H = H_{0;'} + H_{1;'};$$

with

$$H_{0;'} = \sum_k \epsilon_k c_k^\dagger c_k + \sum_q \hbar \omega_q b_q^\dagger b_q + E; \quad (11)$$

$$H_{1;'} = \sum_{k,q} \frac{g_{k,q}}{\sqrt{N}} P b_q^\dagger c_{k+q}^\dagger + b_q c_{k+q}^\dagger c_k; \quad (12)$$

where Fourier transformed operators

$$c_k^\dagger = \frac{1}{\sqrt{N}} \sum_j e^{ikR_j} c_j^\dagger; \quad b_q^\dagger = \frac{1}{\sqrt{N}} \sum_j e^{iqR_j} b_j^\dagger;$$

were introduced. Due to the renormalization processes the one-particle energies ϵ_k and the phonon frequencies ω_q in (11) now depend on the cutoff. Moreover, the phonon energies acquire a dispersion due to an effective interaction of lattice vibrations at different sites via the coupling to electronic degrees of freedom. Also the electron-phonon coupling constant $g_{k,q}$ now depends on wave vectors k, q and the cutoff. E is an additional energy shift. Finally,

the projector P in Eq. (12) guarantees that only those excitations survive in H_1 , which have energies (with respect to H_0) smaller than ϵ :

$$P \left(b_q^y c_{k+q}^y + b_q c_{k+q}^y c_k \right) = \left(j_{q;(\epsilon)}^{\dagger} + n_{k;(\epsilon)}^{\dagger} n_{k+q;(\epsilon)}^{\dagger} \right) b_q^y c_{k+q}^y + b_q c_{k+q}^y c_k : \quad (13)$$

The initial values of the original model (with cutoff $\epsilon = 0$) are

$$n_{k;(\epsilon=0)} = n_k; \quad j_{q;(\epsilon=0)}^{\dagger} = j_0^{\dagger}; \quad g_{k,q;(\epsilon=0)} = g; \quad E_{(\epsilon=0)} = 0 : \quad (14)$$

In the next step we determine the renormalized Hamiltonian $H(\epsilon) = e^X; H e^{-X};$ by eliminating all excitations within an additional small energy shell between (ϵ) and $\epsilon + \delta\epsilon$. For the explicit form of the generator $X;_{\epsilon}$ of the unitary transformation we make the following ansatz

$$X;_{\epsilon} = \frac{1}{N} \sum_{k,q} B_{k,q;(\epsilon)} j_{q;(\epsilon)}^{\dagger} + n_{k;(\epsilon)}^{\dagger} n_{k+q;(\epsilon)}^{\dagger} b_q^y c_k^y c_{k+q}^y + b_q c_{k+q}^y c_k; \quad (15)$$

where $j_{q;(\epsilon)}^{\dagger}(\epsilon)$ is the product of two δ -functions

$$j_{q;(\epsilon)}^{\dagger}(\epsilon) = \left(j_{q;(\epsilon)}^{\dagger} + n_{k;(\epsilon)}^{\dagger} n_{k+q;(\epsilon)}^{\dagger} \right) j_{q;(\epsilon)}^{\dagger}(\epsilon) + n_{k;(\epsilon)}^{\dagger} n_{k+q;(\epsilon)}^{\dagger} j_{q;(\epsilon)}^{\dagger}(\epsilon) : \quad (16)$$

The operator form of $X;_{\epsilon}$ is suggested by its first order expression which is easily obtained by expanding (9) in powers of H_1 and using (10), (cf. Ref. 16). The yet unknown prefactors $B_{k,q;(\epsilon)}$ will be specified later and depend on ϵ . It will turn out that $B_{k,q;(\epsilon)}$ contains contributions in all powers of the electron-phonon coupling g . The two δ -functions in (16) confine the allowed excitations to the energy shell ϵ .

The coefficients $B_{k,q;(\epsilon)}$ will be fixed by the condition (10). First, we have to carry out the unitary transformation (9) explicitly:

$$H(\epsilon) = \sum_k n_k; e^X; c_k^y c_k e^{-X}; + \sum_q j_q^{\dagger}; e^X; b_q^y b_q e^{-X}; + E + \sum_{k,q} \frac{g_{k,q;(\epsilon)}}{N} e^X; P \left(b_q^y c_k^y c_{k+q}^y + b_q c_{k+q}^y c_k \right) e^{-X}; : \quad (17)$$

The transformations for the various operators in (17) has to be done separately. For instance, the transformation for $c_k^y c_k$ reads

$$\begin{aligned} e^X; c_k^y c_k e^{-X}; &= c_k^y c_k = \\ &= \sum_q \frac{j_{q;(\epsilon)}^{\dagger}(\epsilon)}{\hat{n}_{q;(\epsilon)}} \cos(B_{k,q;(\epsilon)} \sqrt{\frac{P}{2\hat{n}_{q;(\epsilon)}}}) \frac{1}{2} (n_{k-q;(\epsilon)}^c + n_{q;(\epsilon)}^b) c_k^y c_{k-q}^y \\ &\quad + \frac{j_{q;(\epsilon)}^{\dagger}(\epsilon) (n_{k-q;(\epsilon)}^c - n_{q;(\epsilon)}^b)}{\hat{n}_{q;(\epsilon)}} \cos(B_{k,q;(\epsilon)} \sqrt{\frac{P}{2\hat{n}_{q;(\epsilon)}}}) \frac{1}{2} b_q^y b_q \\ &\quad + \frac{j_{q;(\epsilon)}^{\dagger}(\epsilon)}{2\hat{n}_{q;(\epsilon)}} \sin(B_{k,q;(\epsilon)} \sqrt{\frac{P}{2\hat{n}_{q;(\epsilon)}}}) b_q^y c_k^y c_{k-q}^y + \text{h.c.} : [k \neq (k+q)] ; \end{aligned} \quad (18)$$

where we have defined

$$n_{k;(\epsilon)}^c = c_k^y c_{k;(\epsilon)=0} = \frac{1}{e^{n_{k;(\epsilon)}} + 1}; \quad n_{q;(\epsilon)}^b = b_q^y b_{q;(\epsilon)=0} = \frac{1}{e^{j_{q;(\epsilon)}} + 1}; \quad (19)$$

and

$$\hat{n}_{q;(\epsilon)} = 1 + 2n_{q;(\epsilon)}^b; \quad (20)$$

(for details see Appendix A). In deriving (18) an additional factorization approximation has been used in order to keep only operators of the structure of those of Eqs. (11) and (12). In principle, the expectation values are best defined with the equilibrium distribution of H since the renormalization step was done from H to H_0 . However, for simplicity we shall evaluate these quantities with the unperturbed Hamiltonian H_0 . Similar expressions to (18) are also found for the transformations of the remaining operators of (17).

One should note that in virtue of the above factorization approximation together with the choice of the equilibrium distribution is not well controlled as long as the influence of the additional fluctuation terms are not considered. However, we believe that the renormalization of H as it is used here leads to a proper description of the influence of the electron-phonon interaction in the Holstein model. The fluctuation terms which appear as additional renormalization contributions in the approach could give rise to additional terms both in H_0 and H_1 . The renormalization of the new coupling parameters would have to be investigated in the present renormalization scheme as well.

In the next step we determine the parameters $B_{k,q}$. For that purpose we use the condition (10). By inserting H_1 from (17) into (10) and by use of (18) and the remaining transformations, we find

$$B_{k,q}(\epsilon) = B_{k,q}(\epsilon) - \frac{1}{2\hbar\omega_q} \arctan \frac{\frac{2\hbar\omega_q}{N} \frac{g_{k,q}}{\omega_q + \epsilon_k - \epsilon_{k+q}}}{\epsilon_k - \epsilon_{k+q}} \quad (21)$$

Let us point out that $B_{k,q}$ is determined by (21) only for the case that the excitation energies $\omega_q + \epsilon_k - \epsilon_{k+q}$ fit into the energy shell given by $B_{k,q}(\epsilon)$. For all other excitations $B_{k,q}$ can be set equal to zero. Therefore we shall use the following expression for $B_{k,q}$:

$$B_{k,q} = \begin{cases} \frac{1}{2\hbar\omega_q} \arctan \frac{\frac{2\hbar\omega_q}{N} \frac{g_{k,q}}{\omega_q + \epsilon_k - \epsilon_{k+q}}}{\epsilon_k - \epsilon_{k+q}} & \text{for } B_{k,q}(\epsilon) = 1 \\ 0 & \text{for } B_{k,q}(\epsilon) = 0 \end{cases}$$

C. Renormalization equations for the Holstein model

Next, we derive the renormalization equations for the parameters of the Hamiltonian. For that purpose we compare the renormalization ansatz for H_1 ,

$$H_1 = \sum_{k,q} \epsilon_{k,q} c_k^\dagger c_k + \sum_q \omega_q b_q^\dagger b_q + E_1 + \sum_{k,q} \frac{g_{k,q}}{N} P(\epsilon_k) (b_q^\dagger c_{k+q}^\dagger + b_q c_{k+q}) \quad (22)$$

[see Eqs. (11) and (12)], with the expression that is obtained from (17) after (18) and the corresponding transformations have been inserted. Comparing in both equations the coefficients of the operators $c_k^\dagger c_k$, $b_q^\dagger b_q$, and $(b_q^\dagger c_{k+q}^\dagger + \text{h.c.})$,

we find the following relations between the parameters at cutoff Λ and (Λ_0) :

$$\begin{aligned}
 \mu_{k;(\Lambda)} &= \mu_{k;(\Lambda_0)} = \\
 &= \sum_q \frac{n_{k+q}^c + n_q^b}{\hbar \omega_q} \cos(B_{k,q}) \frac{1}{2\hbar \omega_q} (1 + \mu_{k,q} + \mu_{k+q}) \mu_{k,q}(\Lambda) \\
 &+ \sum_q \frac{S}{N \hbar \omega_q} \frac{2}{n_{k+q}^c + n_q^b} \sin(B_{k,q}) \frac{1}{2\hbar \omega_q} g_{k,q} \mu_{k,q}(\Lambda) \\
 &+ \sum_q \frac{1}{\hbar \omega_q} \frac{n_k^c + n_q^b}{\hbar \omega_q} \cos(B_{k-q}) \frac{1}{2\hbar \omega_q} (1 + \mu_{k-q} + \mu_k) \mu_{k-q}(\Lambda) \\
 &+ \sum_q \frac{S}{N \hbar \omega_q} \frac{2}{1 - n_k^c + n_q^b} \sin(B_{k-q}) \frac{1}{2\hbar \omega_q} g_{k-q} \mu_{k-q}(\Lambda);
 \end{aligned} \tag{23}$$

$$\begin{aligned}
 \omega_{k;(\Lambda)} &= \omega_{k;(\Lambda_0)} = \\
 &= \sum_k \frac{n_{k+q}^c + n_k^c}{\hbar \omega_q} \cos(B_{k,q}) \frac{1}{2\hbar \omega_q} (1 + \mu_{k,q} + \mu_{k+q}) \mu_{k,q}(\Lambda) \\
 &+ \sum_k \frac{S}{N \hbar \omega_q} \frac{2}{n_{k+q}^c + n_k^c} \sin(B_{k,q}) \frac{1}{2\hbar \omega_q} g_{k,q} \mu_{k,q}(\Lambda);
 \end{aligned} \tag{24}$$

$$\begin{aligned}
 g_{k,q;(\Lambda)} &= g_{k,q;(\Lambda_0)} = \\
 &= \frac{N}{2\hbar \omega_q} (1 + \mu_{k,q} + \mu_{k+q}) \sin(B_{k,q}) \frac{1}{2\hbar \omega_q} \mu_{k,q}(\Lambda) \\
 &+ g_{k,q;(\Lambda_0)} \cos(B_{k,q}) \frac{1}{2\hbar \omega_q} (1 + \mu_{k,q} + \mu_{k+q}) \mu_{k,q}(\Lambda);
 \end{aligned} \tag{25}$$

A corresponding expression can also be found for the renormalization of the energy shift $E_k(\Lambda)$. The above Eqs. (23) to (25) describe the renormalization of the parameters if the cutoff is reduced from Λ to (Λ_0) .

Note that the expression (21) for $B_{k,q}$ and thus the renormalization equations are non-perturbative in $g_{k,q}$ and are not restricted to some low order. However, a prefactor $1/N$ enters the expression (21) for $B_{k,q}$ due to the factorization approximation discussed in Appendix A. Thus, in the thermodynamic limit $N \rightarrow \infty$, $B_{k,q}$ becomes linear in g and the renormalization relations (23) to (25) become quadratic in the electron-phonon coupling. In the numerical evaluation, however, when a fixed number N is taken, the excitation energy $(\omega_{k,q} + \mu_{k,q} + \mu_{k+q})$ will become very small for reducing the cutoff $\Lambda \rightarrow 0$ and thus the expansion of $B_{k,q}$ to linear order in g may break down. In that case the full equations (21) and (23) to (25) have to be taken.

The overall renormalization starts from the cutoff Λ of the original model and proceeds down to zero cutoff $\Lambda_0 = 0$. At $\Lambda_0 = 0$ the completely renormalized Hamiltonian $H^* = H(\Lambda_0)$ becomes an effectively free model and reads

$$H^* = \sum_k \mu_k c_k^\dagger c_k + \sum_q \omega_q b_q^\dagger b_q + E^*; \tag{26}$$

where we have defined $\mu_k = \mu_{k;(\Lambda_0)}$, $\omega_q = \omega_{q;(\Lambda_0)}$, and $E^* = E(\Lambda_0)$. For $\Lambda \rightarrow 0$ the electron-phonon coupling H_1 has vanished due to the δ -function in (13). All excitations of the electron-phonon interaction were used to renormalize the parameters of the Hamiltonian.

The results from the numerical evaluation of the renormalization equations will be given in Sect. IV. In particular we then compare the spectral functions calculated within the PRM approach and by exact diagonalization. The electronic one-particle spectral functions $A_k^+(\omega)$ and $A_k^-(\omega)$ are defined by

$$A_k^+(\omega) = \frac{1}{2} \int_{-\infty}^{\infty} dt \, c_k(t) c_k^\dagger(t) e^{i\omega t}; \quad A_k^-(\omega) = \frac{1}{2} \int_{-\infty}^{\infty} dt \, c_k^\dagger(t) c_k(t) e^{i\omega t}; \tag{27}$$

The function $A_k^+(\omega)$ describes the creation of an electron k at time zero and the annihilation at time t whereas in $A_k(\omega)$ first an electron is annihilated and at time t the electron is created. As is well-known these quantities can be measured by inverse photoemission (IPE) and by photoemission (PE). To evaluate $A_k^+(\omega)$ and $A_k(\omega)$ within the PRM approach it is necessary to unitary transform not only the Hamiltonian but also the operators c_k and c_k^\dagger . This follows from the fact that the trace of any operator quantity is invariant under a unitary transformation. Thus we have to evaluate

$$A_k^+(\omega) = \frac{1}{2} \int_{-1}^1 \langle c_k(t) (c_k^\dagger)^Y \rangle e^{i\omega t} dt; \quad (28)$$

where the expectation value and the time dependence are defined with respect to the ω -dependent Hamiltonian H_ω . Moreover, $(c_k^\dagger)^Y = e^X c_k^\dagger e^{-X}$. A similar expression to Eq. (28) is also valid for $A_k(\omega)$.

In analogy to the evaluation procedure for the renormalization equations of H_ω we make the following ansatz for the ω -dependence of the operators $(c_k^\dagger)^Y$ and $(c_k)^Y$,

$$(c_k^\dagger)^Y = c_k^\dagger + \sum_q \langle c_{k+q}^\dagger \rangle c_{k+q}^\dagger + \langle c_{k+q}^\dagger b_q \rangle c_k^\dagger + \langle c_{k+q}^\dagger b_q^\dagger \rangle c_q^\dagger; \quad (29)$$

$(c_k)^Y = [(c_k)^Y]^Y$, with ω -dependent parameters $\langle c_k \rangle$, $\langle c_{k+q} \rangle$, and $\langle c_{k+q} b_q \rangle$. The parameter values for the original model are

$$\langle c_k \rangle(\omega) = 1; \quad \langle c_{k+q} \rangle(\omega) = 0; \quad \langle c_{k+q} b_q \rangle(\omega) = 0; \quad (30)$$

Due to (29) the following sum rule must hold

$$1 = \langle c_k \rangle + \sum_q \langle c_{k+q} \rangle + \sum_q \langle c_{k+q}^\dagger \rangle \langle c_{k+q} \rangle + \sum_q \langle c_{k+q}^\dagger \rangle \langle c_{k+q} b_q \rangle + \sum_q \langle c_{k+q}^\dagger \rangle \langle c_{k+q} b_q^\dagger \rangle; \quad (31)$$

which follows from the commutator relations. Note that a factorization approximation was used on the right hand side of (31). In analogy to the former approach for $\langle c_k \rangle$, $\langle c_{k+q} \rangle$, and $\langle c_{k+q} b_q \rangle$, we find the following renormalization equations for the parameters $\langle c_k \rangle$, $\langle c_{k+q} \rangle$ and $\langle c_{k+q} b_q \rangle$:

$$\langle c_k \rangle = \sum_q \langle c_{k+q} \rangle \frac{1}{\cos \frac{q}{2} \sqrt{n_{k+q}^c + n_{q,0}^b}} \frac{1}{B_{k+q}} \frac{1}{1 - \langle c_{k+q} \rangle \langle c_{k+q} b_q \rangle}; \quad (32)$$

$$\begin{aligned} & + \sum_q \langle c_{k+q} \rangle \frac{1}{\cos \frac{q}{2} \sqrt{n_k^c + n_{q,0}^b}} \frac{1}{B_{k+q}} \frac{1}{1 - \langle c_{k+q} \rangle \langle c_{k+q} b_q \rangle} \\ & + \sum_q \langle c_{k+q} \rangle \frac{1}{n_{k+q}^c + n_{q,0}^b} \sin \frac{q}{2} \frac{1}{n_{k+q}^c + n_{q,0}^b} \frac{1}{B_{k+q}} \langle c_{k+q} b_q \rangle \langle c_{k+q} \rangle \\ & + \sum_q \langle c_{k+q} \rangle \frac{1}{1 - n_k^c + n_{q,0}^b} \sin \frac{q}{2} \frac{1}{1 - n_k^c + n_{q,0}^b} \frac{1}{B_{k+q}} \langle c_{k+q} b_q \rangle \langle c_{k+q} \rangle; \end{aligned}$$

$$\langle c_{k+q} b_q \rangle = \frac{1}{\cos \frac{q}{2} \sqrt{n_{k+q}^c + n_{q,0}^b}} \sin \frac{q}{2} \frac{1}{n_{k+q}^c + n_{q,0}^b} \frac{1}{B_{k+q}} \langle c_{k+q} \rangle \langle c_{k+q} b_q \rangle; \quad (33)$$

$$\begin{aligned} & + \frac{1}{\cos \frac{q}{2} \sqrt{n_{k+q}^c + n_{q,0}^b}} \frac{1}{B_{k+q}} \frac{1}{1 - \langle c_{k+q} \rangle \langle c_{k+q} b_q \rangle}; \\ & + \cos \frac{q}{2} \frac{1}{1 - n_k^c + n_{q,0}^b} \frac{1}{B_{k+q}} \frac{1}{1 - \langle c_{k+q} \rangle \langle c_{k+q} b_q \rangle}; \end{aligned}$$

and

$$\langle c_{k+q} b_q \rangle = \frac{1}{\cos \frac{q}{2} \sqrt{n_{k+q}^c + n_{q,0}^b}} \sin \frac{q}{2} \frac{1}{1 - n_k^c + n_{q,0}^b} \frac{1}{B_{k+q}} \langle c_{k+q} \rangle \langle c_{k+q} b_q \rangle; \quad (34)$$

$$\begin{aligned} & + \frac{1}{\cos \frac{q}{2} \sqrt{n_{k+q}^c + n_{q,0}^b}} \frac{1}{B_{k+q}} \frac{1}{1 - \langle c_{k+q} \rangle \langle c_{k+q} b_q \rangle}; \\ & + \cos \frac{q}{2} \frac{1}{1 - n_k^c + n_{q,0}^b} \frac{1}{B_{k+q}} \frac{1}{1 - \langle c_{k+q} \rangle \langle c_{k+q} b_q \rangle}; \end{aligned}$$

The renormalization equations (31) and (33) can again be integrated numerically by reducing the cutoff stepwise down to $\Lambda \rightarrow 0$. Together with the Eqs. (23) to (25) the spectral functions (27) can be determined.

$$A_k^+(\omega) = \tilde{\alpha}_k^2(\omega) \tilde{\eta}_k(1 - \tilde{n}_k^c) + \sum_q \tilde{\alpha}_{k;q}^2(\omega + \epsilon_q - \eta_{k+q}) \tilde{n}_q^b(1 - \tilde{n}_{k+q}^c) + \sum_q \tilde{\alpha}_{k;q}^2(\omega - \epsilon_q - \eta_{k-q}) (1 - \tilde{n}_{k-q}^c)(1 + \tilde{n}_q^b); \quad (35)$$

$$A_k(\omega) = \tilde{\alpha}_k^2(\omega) \tilde{\eta}_k \tilde{n}_k^c + \sum_q \tilde{\alpha}_{k;q}^2(\epsilon_q - \eta_{k+q} + \omega) \tilde{n}_{k+q}^c(1 + \tilde{n}_q^b) + \sum_q \tilde{\alpha}_{k;q}^2(\omega - \epsilon_q - \eta_{k-q}) \tilde{n}_{k-q}^c \tilde{n}_q^b; \quad (36)$$

As before, the quantities with tilde denote the parameters at cutoff $\Lambda \rightarrow 0$

$$\tilde{\alpha}_k = \alpha_k(\Lambda \rightarrow 0) \quad \tilde{\alpha}_{k;q} = \alpha_{k;q}(\Lambda \rightarrow 0) \quad \tilde{\alpha}_{k;q} = \alpha_{k;q}(\Lambda \rightarrow 0); \quad (37)$$

In deriving (35) and (36) it was exploited that the completely renormalized Hamiltonian H^* is diagonal [cf. Eq. (26)]. Note that the first parts in $A_k^+(\omega)$ and $A_k(\omega)$ describe the coherent one-electron excitations which correspond to those of a free electron gas. The two remaining contributions are incoherent excitations due to the coupling to phonons and are given by a q -sum over excitations $\eta_{k-q} - \epsilon_q$. Finally we give a sum rule which follows from the frequency integral over the sum of the two spectral functions

$$\begin{aligned} \int_0^\infty d\omega (A_k^+(\omega) + A_k(\omega)) &= \\ &= \tilde{\alpha}_k^2 + \sum_q \tilde{\alpha}_{k;q}^2 (\tilde{n}_{k+q}^c + \tilde{n}_q^b) + \sum_q \tilde{\alpha}_{k;q}^2 (1 + \tilde{n}_q^b - \tilde{n}_{k-q}^c); \end{aligned} \quad (38)$$

Note that Eq. (38) is equivalent to the former relation (31). The explicit evaluation of the spectral functions will be performed in Sect. IV below.

III. EXACT DIAGONALIZATION OF ELECTRON-PHONON MODELS

In principle exact diagonalization techniques allow the analysis of ground-state and spectral properties of microscopic models free of any approximations. However, the vast Hilbert space dimensions restrict ED studies to rather small system sizes, even if state of the art supercomputers are used. Usually the dimension of the matrix involved in the diagonalization is reduced by exploiting lattice or spin symmetries²². Unfortunately, for the Holstein model the Hilbert space associated to the phonons is infinite even for finite systems. Thus a well controlled truncation procedure has to be developed^{21,22}. In our approach the maximum number of phonons per state (not per lattice site!) is fixed (M). Then the dimension of the phononic subspace is $D_{ph} = \frac{(M+N)!}{M!N!}$.

For the Holstein model computational requirements can be further reduced. It is possible to separate the symmetric phonon mode, $B_0 = \frac{1}{\sqrt{N}} \sum_i b_i$, and to calculate its contribution to H analytically. For the sake of simplicity, we restrict ourselves to the 1D case in what follows. Using the momentum space representation of the phonon operators and introducing the polaron binding energy $\epsilon_p = g^2/\omega_0$ the original Holstein Hamiltonian reads

$$H = \sum_{ij} t_{ij} (c_i^\dagger c_j + \text{h.c.}) - \epsilon_p \sum_j \left(\sum_i B_{Q_j}^\dagger + B_{Q_j} \right) n_{Q_j} + \sum_j \omega_0 B_{Q_j}^\dagger B_{Q_j} \quad (39)$$

with

$$B_{Q_j}^\dagger = \frac{1}{\sqrt{N}} \sum_i U_{ji} b_i^\dagger; \quad B_{Q_j} = \frac{1}{\sqrt{N}} \sum_i U_{ji} b_i = \sum_i U_{ji} b_i; \quad (40)$$

$$n_{Q_j} = \sum_i U_{ji} n_i; \quad (41)$$

where $U_{ji} = \frac{1}{\sqrt{N}} \exp(iQ_j R_i)$. Q_j (R_i) denote the allowed momentum (translation) vectors of the lattice. The phononic $Q = 0$ mode couples to $n_0 = \frac{N+1}{N}$ which is a constant if working in a subspace with fixed number of

electrons. Thus the Hamiltonian decomposes into $H = H^e + H_{Q=0}$, with

$$H_{Q=0} = \sum_p \frac{1}{p!} (B_0^y + B_0) n_0 + \sum_0 B_0^y B_0 : \quad (42)$$

Since $[H^e; H_{Q=0}] = 0$ holds the eigenspectrum of H can be built up by the analytic solution for $H_{Q=0}$ and the numerical results for H^e . Using the unitary transformation

$$S(N_{el}) = \exp \left[\sum_p \frac{N_{el}}{p!} \frac{1}{p!} (B_0^y - B_0) \right] ; \quad (43)$$

and introducing a shift of the phonon operators $(B_0 \rightarrow B_0 + \sum_{el} \frac{N_{el}}{p!} \frac{1}{p!})$, we easily find the diagonal form of $H_{Q=0}$

$$H_{Q=0} = \sum_0 B_0^y B_0 + \sum_p \frac{N_{el}^2}{p!} ; \quad (44)$$

It represents a harmonic oscillator with eigenvalues and eigenvectors:

$$E_1 = \sum_0 1 + \sum_p \frac{N_{el}^2}{p!} ; \quad (45)$$

$$|i\rangle = \sum_{el} \frac{1}{p!} (B_0^y)^p |i\rangle ; \quad (46)$$

The corresponding eigenenergies and eigenvectors of $H_{Q=0}$ are $E_1 = E_1$ and

$$|i; N_{el}\rangle = S^y(N_{el}) |i\rangle ; \quad (47)$$

respectively. That is, in the eigenstates of the Holstein model a homogeneous lattice distortion occurs. Note that the homogeneous lattice distortions are different in subspaces with different electron number. Thus excitations due to lattice relaxation processes show up in the one-particle spectral function. Finally, eigenvectors and eigenenergies of H can be constructed by combining the above analytical result with the numerical determined eigensystem $(\tilde{E}_n^{(N_{el})}; \tilde{j}_n^{(N_{el})})$ of H^e :

$$E_{n;l}^{(N_{el})} = \tilde{E}_n^{(N_{el})} + \sum_0 1 + \sum_p \frac{N_{el}^2}{p!} ; \quad (48)$$

$$|j_{n;l}^{(N_{el})}\rangle = |\tilde{j}_n^{(N_{el})}\rangle |j; N_{el}\rangle ; \quad (49)$$

The direct product notation for the eigenvectors of H implies that also the one-particle spectral functions, e.g. the single-particle spectral function

$$A_K^+(\omega) = \sum_{n;l} \langle j_{n;l}^{(N_{el}+1)} | \hat{c}_K^\dagger | j_{0;0}^{(N_{el})} \rangle \langle j_{0;0}^{(N_{el})} | \hat{c}_K | j_{n;l}^{(N_{el}+1)} \rangle ; \quad (50)$$

can also be decomposed in a numerical and an analytical contribution:

$$A_K^+(\omega) = \sum_l (l; N_{el} + 1; N_{el}) A_K^+(\omega - [\sum_0 1 + \sum_p (2N_{el} + 1) \frac{N_{el}^2}{p!}]) ; \quad (51)$$

Using ED in combination with kernel polynomial moment expansion and maximum entropy methods^{22,23,24}, we first compute numerically the one-particle spectral function for H^e ,

$$\tilde{A}_K^+(\omega) = \sum_n \langle \tilde{j}_n^{(N_{el}+1)} | \hat{c}_K^\dagger | \tilde{j}_0^{(N_{el})} \rangle \langle \tilde{j}_0^{(N_{el})} | \hat{c}_K | \tilde{j}_n^{(N_{el}+1)} \rangle ; \quad (52)$$

which does not include the effects of the $Q = 0$ phonon mode. In a second step, the final spectrum is constructed from Eq. (51) by shifting $\tilde{A}_K^+(\omega)$ by multiples of the bare phonon frequency and using the weight factors²⁵

$$(l^0; N_{el}^0; N_{el}) = \langle j(N_{el}^0; l^0) | j(N_{el}) \rangle^2 = \frac{x^{l^0}}{l^0!} e^{-x} ; \quad (53)$$

where $x = \frac{1}{N} \sum_{\mathbf{k}} (N_{\text{el}}^0 - N_{\text{el}})^2$. The $(l^0; N_{\text{el}}^0; N_{\text{el}})$ quantify the relaxation process of the lattice distortion discussed above. Thus, each excitation in $A_K^+(\mathbf{k})$ splits up into a band of peaks separated by ω_0 which contains the total weight of the original excitation $[\sum_{\mathbf{l}} (l^0; N_{\text{el}} + 1; N_{\text{el}}) = 1]$.

Fig. 1 shows the contribution of the $Q = 0$ phonon mode to $A_K^+(\mathbf{k})$. The $Q = 0$ excitations are separated by ω_0 and interfere at higher energies with excitations forming broad bands. In Fig. 1, e.g., five replications of the lowest peak are visible (with decreasing height and weight). The integrated spectral density reflects the redistribution of spectral weight to higher energies but conserves the spectral weight when integrating the $Q \neq 0$ peaks together with the corresponding $Q = 0$ side bands. Note that this behavior is observed in a finite system only, i.e., $(l^0 = 1; N_{\text{el}} = 1; N_{\text{el}})$ vanishes in the thermodynamic limit $N \rightarrow \infty$.

In our finite cluster diagonalization, however, the separation of the phononic $Q = 0$ mode significantly reduces the computational requirements. First, the dimension of the matrix to be diagonalized is reduced by a factor of $1 + \frac{M}{N}$ because only $N - 1$ instead of N independent modes have to be considered. Second, the $Q = 0$ mode takes into account at least $\hbar \sum_{\mathbf{k}} \omega_{\mathbf{k}} = \frac{\omega_0}{\omega_0} \sum_{\mathbf{k}} \omega_{\mathbf{k}}$ phonons in the ground state already. Thus, the maximum number of phonons allowed per state, M , can be chosen much smaller for H than for the full Hamiltonian H in order to achieve the same level of convergence. The relevance of the separation of the phononic $Q = 0$ mode for our numerical work becomes evident if one compares the dimension of the phononic Hilbert space used for the calculation in Fig. 1 ($N_{\text{el}} = 4; N - 1 = 7; M = 28; \omega_{\mathbf{k}} = \omega_0 = 6$) $D_{\text{ph}} = 6 \cdot 7 \cdot 10^6$ with that required for the full Hamiltonian ($N = 8; M = 28 + 12$) $D_{\text{ph}} = 3 \cdot 7 \cdot 10^8$, which is about two orders of magnitude larger.

IV. PEIERLS TRANSITION IN THE SPINLESS FERMION HOLSTEIN MODEL

In this section we apply the PRM and ED techniques outlined in Secs. II and III to the investigation of the metal-insulator transition in the Holstein model. While both approaches are valid for any dimension in principle, we restrict ourselves to the one-dimensional case and spinless fermions, mainly because of the serious memory restrictions within the ED calculations. On the other hand, focusing on the half-filled band case $N_{\text{el}} = N/2$, we know that the Peierls instability, we are interested in, is most pronounced in low-dimensional systems. Throughout the numerical work we use the bare tight-binding electron dispersion $\epsilon_{\mathbf{k}} = -2t \cos ka$ (lattice constant $a = 1$), and an Einstein phonon frequency $\omega_0 = t = 0.1$. The Fermi level is defined to be the energy zero level and the temperature is $T = 0$. In the following we shall vary the dimensionless electron-coupling constant $g = t$ or, equivalently, $\omega_p = t$ [where due to $g = \sqrt{\frac{N}{N_{\text{el}}}} \omega_p$ we have $\omega_p = t = (g = t)^2$ ($t = \omega_0$)].

A. ED results

In order to investigate lattice dynamical effects on the Peierls transition we first analyze the spectral density of single-particle excitations associated with the injection of an electron with wave number K , $A_K^+(\mathbf{k})$ (IPE), given by Eq. (50), and the corresponding quantity for the emission of an electron, $A_K^-(\mathbf{k})$ (PE). In $A_K^+(\mathbf{k})$ the destruction operator $c_{\mathbf{k}}$ connects the ground state of the Holstein model with N_{el} electrons ($|j_{0,0}^{(N_{\text{el}})}\rangle$) to all excited states of the system with $N_{\text{el}} - 1$ electrons ($|j_{n,l}^{(N_{\text{el}}-1)}\rangle$). Of course, the exact determination of $A_K^+(\mathbf{k})$ for coupled electron-phonon systems is an tremendous numerical task, which requires the repeated solution of eigenvalue problems with dimensions of the order of 10^{10} . At present this can only be achieved by employing elaborate numerical techniques, e.g. the kernel polynomial expansion method, on leading edge supercomputers.²⁶

Let us first consider the adiabatic ($\omega_0 = 0$) weak coupling regime $\omega_p = t = 1$. The data presented for the single-particle spectral function in Fig. 2 give clear evidence that the system behaves like a metal. The Fermi energy ($K_F = \pi/2$) is located in the center of an only weakly renormalized band (the bandwidth is about $4t$, which is the value for noninteracting system). The band dispersion can be derived by tracing the lowest (uppermost) peak in each K sector of the IPE (PE) spectra. Most notably these peaks have a spectral weight close to one. As an effect of the electron-phonon coupling phonon satellites separated by the bare phonon frequency $\omega_0 = t$ occur in the vicinity of the tight-binding band electron levels. These excitations, however, have extremely small (electronic) spectral weight.

If we increase the electron-phonon interaction a gap feature starts to develop in the single-particle spectra at the Fermi momentum. This is the situation shown in Fig. 3. Obviously a critical interaction strength is necessary to trigger the Peierls transition at finite phonon frequencies. This has to be contrasted to the result obtained for the adiabatic limit $\omega_0 = 0$, where a Peierls instability occurs at any finite electron-phonon coupling. Figure 3 also demonstrates the mixed (electron-phonon) nature of the excitations. Now the spectral weight is almost equally distributed among the different peaks in each K sector.

Finally we examine the behavior of the single-particle spectra in the strong electron-phonon coupling regime. As can be seen from Fig. 4, a wide band gap emerges, indicating massive charge excitations accompanied by multiphonon absorption and emission processes. The Peierls distortion of the lattice is directly connected to a charge-density-wave formation (we found almost localized electrons at every second site). As a result a symmetry-broken ground state may occur in the infinite system, reflecting true long-range order. Now the Fermi energy is located at the center of the band gap and consequently the system shows insulating behavior.

To supplement the discussion we display in Fig. 5 the contribution of states with m phonons contained in the ground state. From top to the bottom the coupling strength increases. At weak electron-phonon coupling " $\mu = 0.1$ " the zero-phonon state is clearly the dominant one. States with more than two phonons are negligible. For the Peierls phase (" $\mu = 1.6$ ") the phonon distribution of the ground state follows a Poisson-like distribution, where the ratio " $\mu = 1.6$ " gives a good estimate of the mean phonon number.

B. PRM results

In order to integrate the renormalization equations derived in Sec. II we consider a lattice of $N = 1000$ sites in one dimension. The width of the energy shell was taken to be somewhat smaller than the typical smallest energy spacing of the eigenstates of H_0 . Fig. 6 shows the electronic spectral functions $A_k^+(\omega)$ and $A_k^-(\omega)$ [calculated from Eqs. (35) and (36)], and the renormalized phonon dispersion ω_q from the PRM approach for a g -value of $g = \mu = 0.10$ (" $\mu = 0.1$ ") which is below the critical electron-phonon coupling g_c . The wave number k is fixed to $k_F = \pi/2$. Note that for g values smaller than g_c the system is in a Luttinger liquid (metallic) phase. As is seen from Fig. 6 the one-particle spectrum consists of a main pole and of satellites due to the coupling of the electrons to phonons. They follow from the first and to the second and third terms on the r.h.s. of Eqs. (36) and (37) and will be denoted in the following as coherent and incoherent excitations. Note that due to the used approximations to derive the PRM equations it is beyond the scope of the present approach to discuss possibly differences between a Luttinger liquid and a Fermi liquid behavior in the one-particle spectral functions.

As was mentioned before we restrict ourselves to $k = k_F$. Therefore the coherent excitation is located at the Fermi level [dotted line in Fig. 6 (a)]. It is the dominant excitation of the spectrum since its pole strength $\sim \omega_{k_F}^2$ is close to its maximum value of 1. Due to (38) the intensity sum over all coherent and incoherent excitations is equal to 1. The system is in a metallic state. Note the small finite onset of the incoherent parts in $A_k^+(\omega)$ and $A_k^-(\omega)$ close to the Fermi level which is due to the finite phonon frequency $\omega_q \neq 0$ (for small g -values). In Fig. 6 (b) the renormalized phonon frequency ω_q is shown as a function of the wave number. Due to the coupling between the phononic and the electronic degrees of freedom, ω_q has gained some dispersion. For the chosen g value this dispersion is relatively small except for wave numbers q close to the Brillouin-zone center and close to the Brillouin-zone boundary ($k_0 = \pi$). This feature can be understood from the phonon renormalization equation (24). There, the second order renormalization contribution corresponds to a frequency dependent energy shift which is similar to that known from the phonon self-energy contribution of second order. The dispersion results from particle-hole excitations $c_k^\dagger c_{k+q}$ around the Fermi level with a wave number transfer q which is either small ($q \rightarrow 0$) or about $q = k_F$ (since at half-filling " $k_F = \pi/2$ "). Note that Fig. 6 shows an overall agreement with the ED results of Fig. 2 where the same parameter have been used.

In Fig. 7 a) and b) the same quantities are shown for $g = \mu = 0.30$ (" $\mu = 0.3$ "). In this case the coupling strength is somewhat below the critical value g_c . This can be seen from the pole strength $\sim \omega_{k_F}^2$ of the coherent pole which has considerably decreased from almost 1 to a value already very small compared to 1. Since the vanishing of $\omega_{k_F}^2$ has to be interpreted as a signature of the metal-insulator transition the system is still in the metallic state. In Fig. 7 b) the renormalized phonon frequency ω_q is shown. For large wave numbers approaching the Brillouin-zone boundary a strong softening is observed. Only for wavevectors extremely close to the boundary a sudden stiffening is found again. This feature is reminiscent of the behavior at k_0 discussed before.

This stiffening is absent in Fig. 8 b) where the PRM result for the renormalized phonon frequency is shown for $g = \mu = 0.34$ (" $\mu = 1.156$ ") which is somewhat larger than the critical g value (within the PRM approach). In this case the phonon excitation becomes negative very close to the Brillouin-zone boundary k_0 . The negative phonon frequency indicates the occurrence of an instability at the critical coupling strength g_c which is associated with the transition of the system to a Peierls state. Note that for $g > g_c$ the present PRM treatment breaks down since a possible shift of the ionic equilibrium positions was not taken into account. A discussion of the phonon dynamics in the Peierls state will be subject to further research. However, in contrast to the discussion of the phonon modes the discussion of the electronic excitations within the PRM method is not restricted to g values $g < g_c$ but can be extended to some small range above g_c (see below). In Fig. 8 a) the spectral functions $A_k^+(\omega)$ and $A_k^-(\omega)$ from the PRM treatment are shown

for the same g value $g=t=0.34$. The spectrum has changed from a strongly peaked distribution for smaller g to a more Poisson-like shape. The coherent pole has completely vanished $\sim_{k_F}^2 = 0$ and a gap has opened in the spectrum at the Fermi level. The system has undergone a phase transition to a nonmetallic state. To verify that the gap does not depend on the lattice size we have applied the PRM to a rather large system with 1000 sites but also to smaller systems with 800, 500, 200, and 100 sites. In all cases the size of the gap was practically independent of the system size so that the gap can be considered as an intrinsic property of the Holstein model. As in any renormalization group procedure the results could depend on the actual cluster size due to additional degeneracies imposed by symmetry, especially for small systems. Such a dependence was not found for the systems considered here.

To find the critical coupling strength at which the phase transition occurs we have plotted the coherent pole strength $\sim_{k_F}^2$ at wave vector $k = k_F$ for different values of g (Fig. 9). Note the strong decrease of $\sim_{k_F}^2$ with increasing g . A closer inspection of the data shows that at $g = g_c = 0.31$ the pole strength becomes zero which marks the transition of the system to the nonmetallic state. This value is somewhat larger than the critical value found from the exact diagonalization [$g_c=t=0.24$ ($t_p=t=0.6$), compare Fig. 3]. Note, however, that in the PRM approach a rather large system with 1000 lattice sites was used, whereas in the ED the system had to be restricted to 8 sites. For the smaller systems with 800;500;300;200, and 100 sites the critical coupling was slightly smaller and approximately $g_c=t=0.30$. A comparison with the critical value $g_c=t=0.28$, obtained from DMRG calculations of Refs. 12,13, shows that the critical values from PRM might be somewhat too large. The difference is probably due to the factorization approximation in the PRM approach and to the simplified ansatz (15) for the operator form of the generator X ; .

An alternative criterion to determine the critical coupling strength is to take that value at which the renormalized phonon frequency ω_q at the Brillouin-zone boundary $q = k_0$ vanishes. In this way one finds for the system with 1000 sites $g_c=t=0.30$, i.e., a result which is somewhat smaller than that found from the vanishing of $\sim_{k_F}^2$. Note however that the latter g_c value seems to be the more reliable one. This can be understood from the comparison of the renormalization equations (32) for k_i and (24) for ω_{q_i} . As can be seen, for k_i an approximate exponential decay with i is found whereas a logarithmic decay follows for ω_{q_i} . Thus, since the dominant renormalization contributions always occur at small i , the numerical errors are much smaller for k_i than for ω_{q_i} . Therefore, within the present renormalization approach the critical coupling strength found from the vanishing of the coherence strength $\sim_{k_F}^2$ is probably more reliable than that given by the vanishing of $\omega_{q=k_0}$. On the other hand, from comparison with other approaches one has to admit that the value of $g_c=t=0.31$ is possibly somewhat too large probably due to the factorization approximation which was used to derive the renormalization equations.

As was mentioned above, the PRM approach is only valid in the metallic regime $g < g_c$. However, one can assure oneself of the fact that it may also be applied in a small parameter regime $g > g_c$: We again consider $k = k_F$. Due to the $\omega_{k,q}$ -functions in all renormalization equations a renormalization approximately occurs when the energy difference $\omega_{q_i} + \omega_{k_i} - \omega_{k+q_i}$ lies within a small energy shell between ω_{k_F} and $\omega_{k_F+k_0}$. Moreover, the most dominant renormalization processes take place for small i . Therefore, $\omega_{k_F+q_i} - \omega_{k_F}$ has to be fulfilled (where a small phonon frequency was assumed). It follows that $q = k_0$, where k_0 is the zone-boundary wave vector. According to (32) the coherent pole strength $\sim_{k_F}^2$ will mostly be renormalized by wave numbers $q = k_0$. In contrast $\omega_{k_F+k_0}$ and $\omega_{k_F-k_0}$ are both renormalized only once when i is small. According to (32) ω_{k_F} becomes zero for small i in the insulating regime $g > g_c$, so that the renormalization of $\omega_{k_F+k_0}$ and $\omega_{k_F-k_0}$ is negligible due to (33) and (34). Note that the incoherent excitations in (35) and (36) close to $q = k_0$ contain negative phonon energies ω_{q_i} . However, they do not influence the electronic spectral functions.

V. SUMMARY

In this paper the electron-phonon coupling in the one-dimensional Holstein model at half-filling has been investigated using both the projector-based renormalization method (PRM) and an refined exact diagonalization technique in combination with the kernel polynomial method (ED). In this system a metal-insulator transition occurs, accompanied by the formation of Peierls distorted state. This transition has been analyzed in terms of the (inverse) photoemission spectral functions, where the phonon dynamics is fully taken into account.

Different from the ED the present PRM treatment is restricted to values g smaller or equal to the critical electron-phonon coupling g_c . The discussion of the coupling regime g larger than g_c is more complicated and has to be postponed to a future investigation. However, it turns out that the results for the electronic spectral functions are not restricted to $g < g_c$ but are also valid in a small regime g above g_c . Therefore, the opening of an electronic gap can be observed. The reason is that electronic properties are rather insensitive against a small number of unstable phonon modes close to the Brillouin-zone boundary.

Although both the PRM and the ED technique are valid for any dimension, we have restricted ourselves to a one-dimensional lattice. The (inverse) photoemission spectral functions from both approaches clearly indicate a metal-insulator transition and the opening of a gap if the electron-phonon coupling becomes larger than a finite critical value. The single-particle spectra excitations are accompanied by multiphonon absorption and emission processes in the Peierls phase. The PRM provides a renormalized phonon dispersion which shows a softening at the Brillouin-zone boundary. This effect even occurs for coupling strength g smaller than the critical value g_c so that the phonon softening can be understood as a precursor effect of the gap formation.

Acknowledgements

We appreciate valuable discussions with A. R. Bishop, K. Meyer, T. Sommer, and A. Weide. Work in Dresden, Davis, Erlangen and Greifswald was partially supported by the Deutsche Forschungsgemeinschaft through the research programs SFB 463, under Grant No. HU 993/1-1, the Bavarian Competence Network for High Performance, and SPP 1073, respectively. Special thanks go to the HLRN Berlin-Hannover, RRZ Erlangen, and LRZ Muenchen for the generous granting of their computer facilities.

APPENDIX A: TRANSFORMATION OF THE OPERATORS

In this appendix we evaluate the transformation from () to (). As an example let us consider the operator $c_k^y c_k$

$$e^X ; c_k^y c_k e^{-X} ; = e^X ; c_k^y c_k = \sum_{n=0}^X \frac{1}{n!} X^n ; c_k^y c_k \quad (A1)$$

Here, a new super-operator $X ;$ was introduced which is defined by the commutator of the generator $X ;$ with operators A on which $X ;$ is applied, $X ; A = [X ; A]$. Thus we have to evaluate the commutators on the r.h.s. of (A1)

$$[X ; ; c_k^y c_k] = \frac{1}{N} \sum_q X^n B_{k-q;q} (;) b_q^y c_{k-q}^y c_k + b_q c_{k-q}^y c_k \quad (A2)$$

By applying $X ;$ twice on $c_k^y c_k$ products composed of four fermionic and of two fermionic and two bosonic operators occur. In order to keep only operators which are also present in $H ()$, a factorization is performed. One obtains

$$\begin{aligned} \frac{1}{2} [X ; ; [X ; ; c_k^y c_k]] = \\ = \frac{1}{N} \sum_q X^n B_{k-q;q}^2 (;) (n_k^c + n_{q;}^b) c_{k-q}^y c_k \\ + B_{k-q;q}^2 (;) (1 - n_{k-q;}^c + n_{q;}^b) c_k^y c_{k-q} \\ + B_{k-q;q}^2 (;) (n_{k-q;}^c - n_k^c) b_q^y b_q + [k ! k + q] \end{aligned} \quad (A3)$$

where the expectation values $n_k^c, n_{q;}^b$ have been defined in (19). The third order term of (A1) again gives interaction-type contributions. Thus, all operator terms appearing on the r.h.s. of (A1) are traced back to those which also appear in H . This property enables us to evaluate all higher order commutators with $X ;$ and thus the transformation (A1). the result is given in (18).

¹ A. Lanzara, P. V. Bogdanov, et al., Nature 412, 510 (2001).

² O. Gunnarsson, Rev. Mod. Phys. 69, 575 (1997).

³ A. J. Millis, P. B. Littlewood, and B. I. Shraiman, Phys. Rev. Lett. 74, 5144 (1995).

- ⁴ A . R . B ishop and B . I . Swanson, *Los A lam os Science* 21, 133 (1993); N . T suda, K . N asu, A . Y anese, K . S iratori, *Electronic Conduction in Oxides* (Springer-Verlag, Berlin, 1991); *Organic Conductors*, edited by J . P . Farges, (M arcel D ekker, New York 1994).
- ⁵ J . E . H irsch and E . F radkin, *Phys. Rev. B* 27, 4302 (1983).
- ⁶ G . B enfatto, G . G alliovotti, and J . L . Lebow itz, *Helv. Phys. Acta* 68, 312 (1995).
- ⁷ H . Fehske, G . W ellein, G . H ager, A . W ei e, K W . Becker, and A . R . B ishop, *cond-m at/0406023*.
- ⁸ H . Zheng, D . Feinberg, and M . A vignon, *Phys. Rev. B* 39, 9405 (1989).
- ⁹ L . G . Caron and C . B ourbonnais, *Phys. Rev. B* 29, 4230 (1984).
- ¹⁰ R . H . M cK enzie, C . J . H am er, and D . W . M urray, *Phys. Rev. B* 53, 9676 (1996).
- ¹¹ A . W ei e and H . Fehske, *Phys. Rev. B* 58, 13526 (1998); H . Fehske, M . H ollicki, and A . W ei e, *Advances in Solid State Physics* 40, 235 (2000).
- ¹² R . J . B ursill, R . H . M cK enzie, and C . J . H am er, *Phys. Rev. Lett.* 80, 5607 (1998).
- ¹³ H . Fehske, G . W ellein, G . H ager, A . W ei e, and A . R . B ishop, *Phys. Rev. B* 69, 165115 (2004).
- ¹⁴ E . J eckelmann, C . Zhang, and S . R . W hite, *Phys. Rev. B* 60, 7950-7955 (1999).
- ¹⁵ D . M eyer, A . C . H ewson, and R . Bulla, *Phys. Rev. Lett.* 89, 196401 (2002).
- ¹⁶ K . W . Becker, A . H ubsch, and T . Som mer, *Phys. Rev. B* 66, 235115 (2002).
- ¹⁷ F . W egner, *Ann. Phys. (Leipzig)* 3, 77 (1994).
- ¹⁸ S . D . G lazek and K . G . W ilson, *Phys. Rev. D* 48, 5863 (1993); S . D . G lazek and K . G . W ilson, *Phys. Rev. D* 49, 4214 (1994).
- ¹⁹ A . H ubsch and K W . Becker, *Eur. Phys. J. B* 33, 391 (2003).
- ²⁰ A . H ubsch and K W . Becker, *cond-m at/0406653*.
- ²¹ Y . Inada and C . Ishii, *J. Phys. Soc. Jpn.* 59, 612 (1990).
- ²² B . Baum l, G . W ellein, and H . Fehske, *Phys. Rev. B* 58, 3663 (1998).
- ²³ R . N . Silver, H . Roder, A . F . Voter, and J . D . K res, *Int. J. Mod. Phys. C* 124, 115 (1996).
- ²⁴ R . N . Silver and H . Roder, *Phys. Rev. E* 56, 4822 (1997).
- ²⁵ J . M . Robin, *Phys. Rev. B* 56, 13 634 (1997).
- ²⁶ G . W ellein and H . Fehske, in *High Performance Computing in Science and Engineering '99* edited by E . K rause and W . Jager, Springer-Verlag Berlin Heidelberg (2000), pp. 112-129; H . Fehske, G . W ellein, A . P . K am pf, M . Sekania, G . H ager, A . W ei e, H . Buttner, and A . R . B ishop, in *High Performance Computing in Science and Engineering*, Munich 2002, edited by S . W agner, W . Hanke, A . Bode, F . D urst, Springer-Verlag Berlin Heidelberg (2003), pp 339-349.

FIG. 1: Low-energy excitations of the single-particle spectral function $A_K^+(\omega)$ and the corresponding integrated spectral density $S_K^+(\omega) = \int_0^\omega A_K^+(\omega') d\omega'$ at $K = \pi/2$ for $t_p = t = 0.6$ and $t_o = t = 0.1$. Dashed (solid) lines show the spectrum including all phonon modes (without the $Q = 0$ phonon mode).

FIG. 2: (Color online) Wave-number-resolved spectral densities for photoemission $A_K^+(\omega)$; dashed (red) lines] and inverse photoemission $A_K^-(\omega)$; solid (black) lines] in the metallic state ($t_p = t = 1$). The corresponding integrated densities $S_K^+(\omega)$ are given by bold lines. ALBED data were obtained for an eight-site system with periodic boundary conditions. Note that the sum rules are fulfilled.

FIG. 3: (Color online) PE [dashed (red) lines] and IPE [solid (black) lines] spectra near the metal to Peierls insulator transition point.

FIG. 4: (Color online) PE and IPE spectra in the Peierls phase.

FIG. 5: (Color online) Phonon distribution in the ground state of the spinless Holstein model for three characteristic coupling strengths.

FIG. 6: Results from the PRM approach for $g=t = 0.10$ ($\mu_p=t = 0.1$): (a) Electronic spectral functions $A_k^+(\omega)$ (black) and $A_k^-(\omega)$ (red) where the wave number k is fixed to $k_F = \pi/2$. The coherent excitation peak (dotted line) is at $\omega = 0$. (b) Renormalized phonon dispersion ω_q . The original phonon frequency is $\omega_0=t = 0.1$.

FIG. 7: Same quantities as in Fig. 6 from the PRM approach for a g -value of $g/t = 0.30$ ($\mu_p/t = 0.9$) somewhat below the critical value $g_c/t = 0.31$ ($\mu_p/t = 0.96$).

FIG. 8: Same quantities as in Fig. 6 from the PRM approach for $g/t = 0.34$ ($\mu_p/t = 1.16$) which is somewhat larger than $g_c/t = 0.31$ ($\mu_p/t = 0.96$). Note that the coherent pole has vanished and a charge gap has opened (Fig. 8 a))

FIG. 9: Coherent pole strength $\sim \kappa_F^2$ from the PRM approach as function of the electron-phonon coupling g for a system with 1000 lattice sites

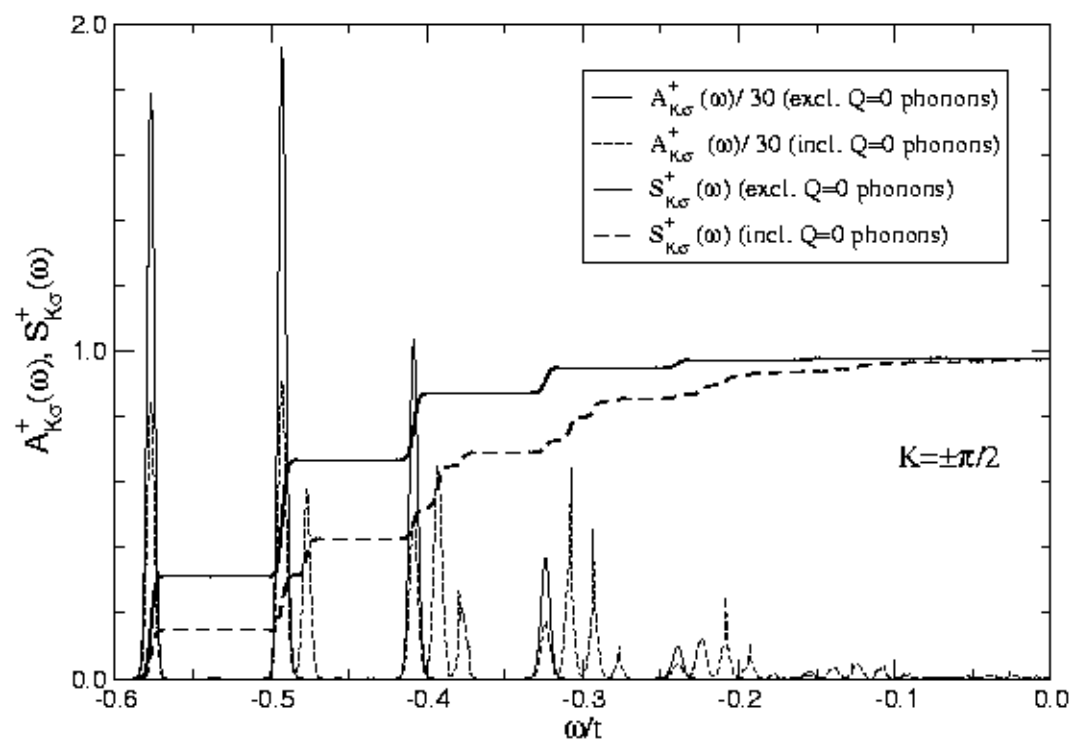


Fig. 1

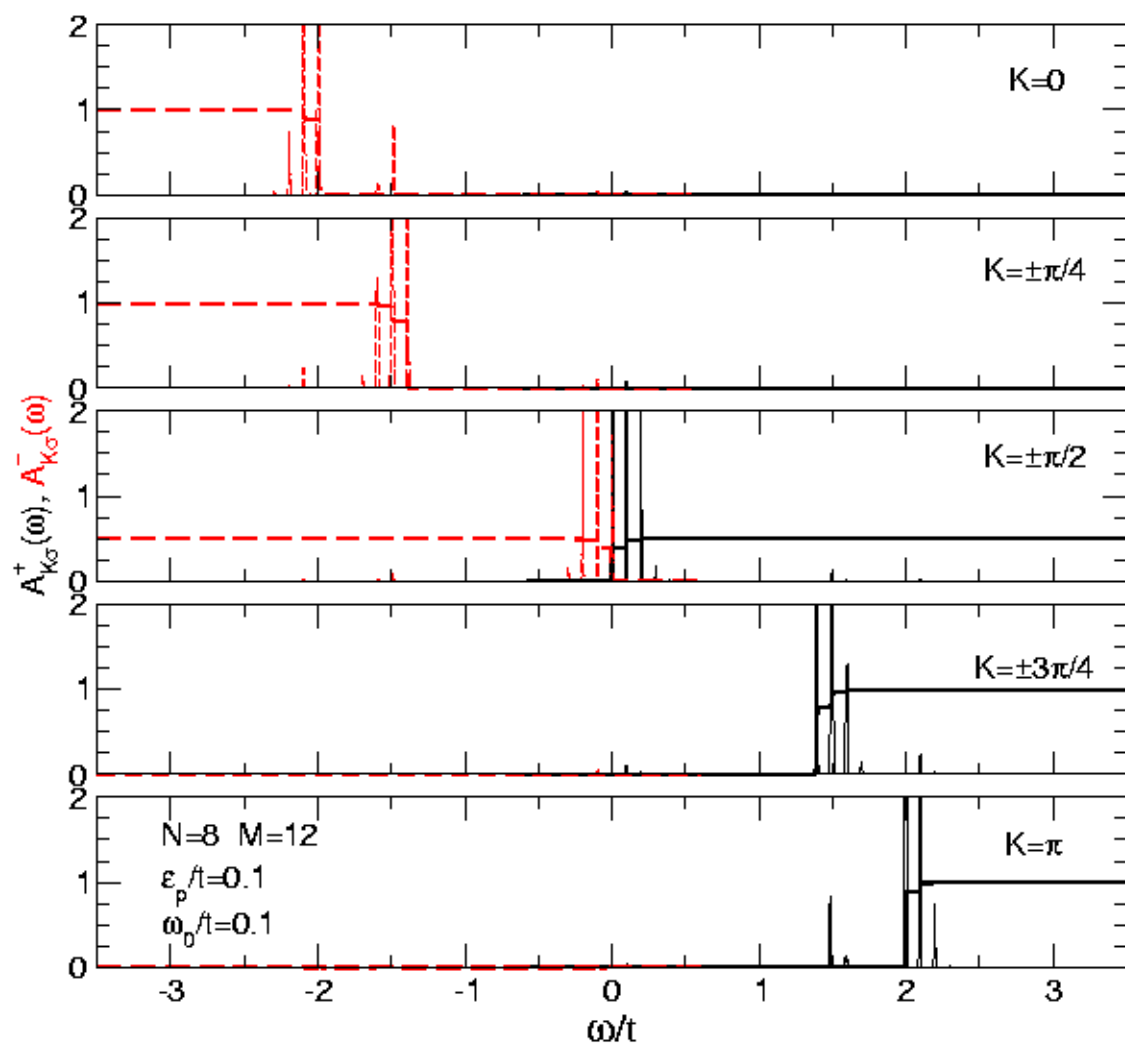


Fig. 2

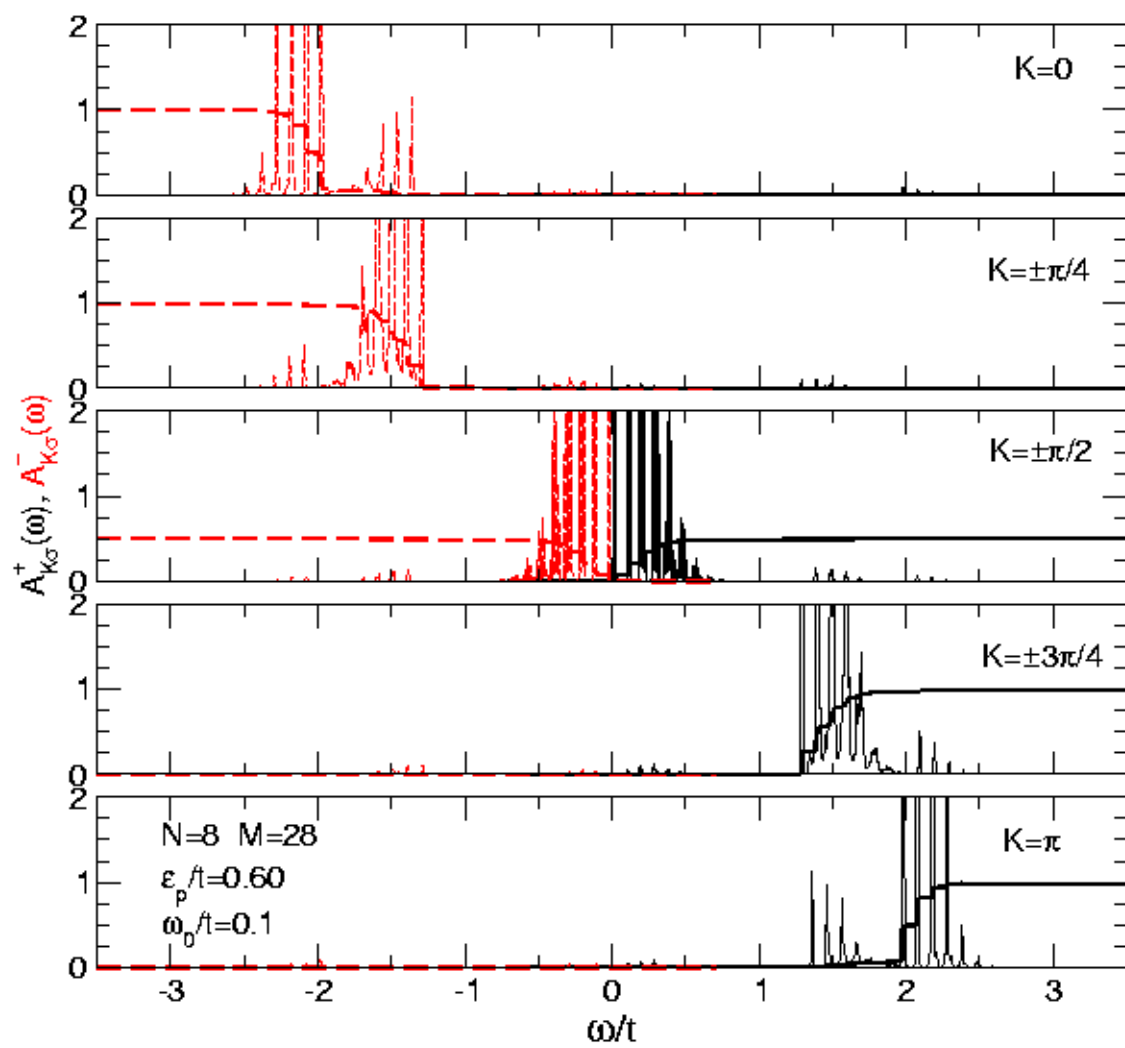


Fig. 3

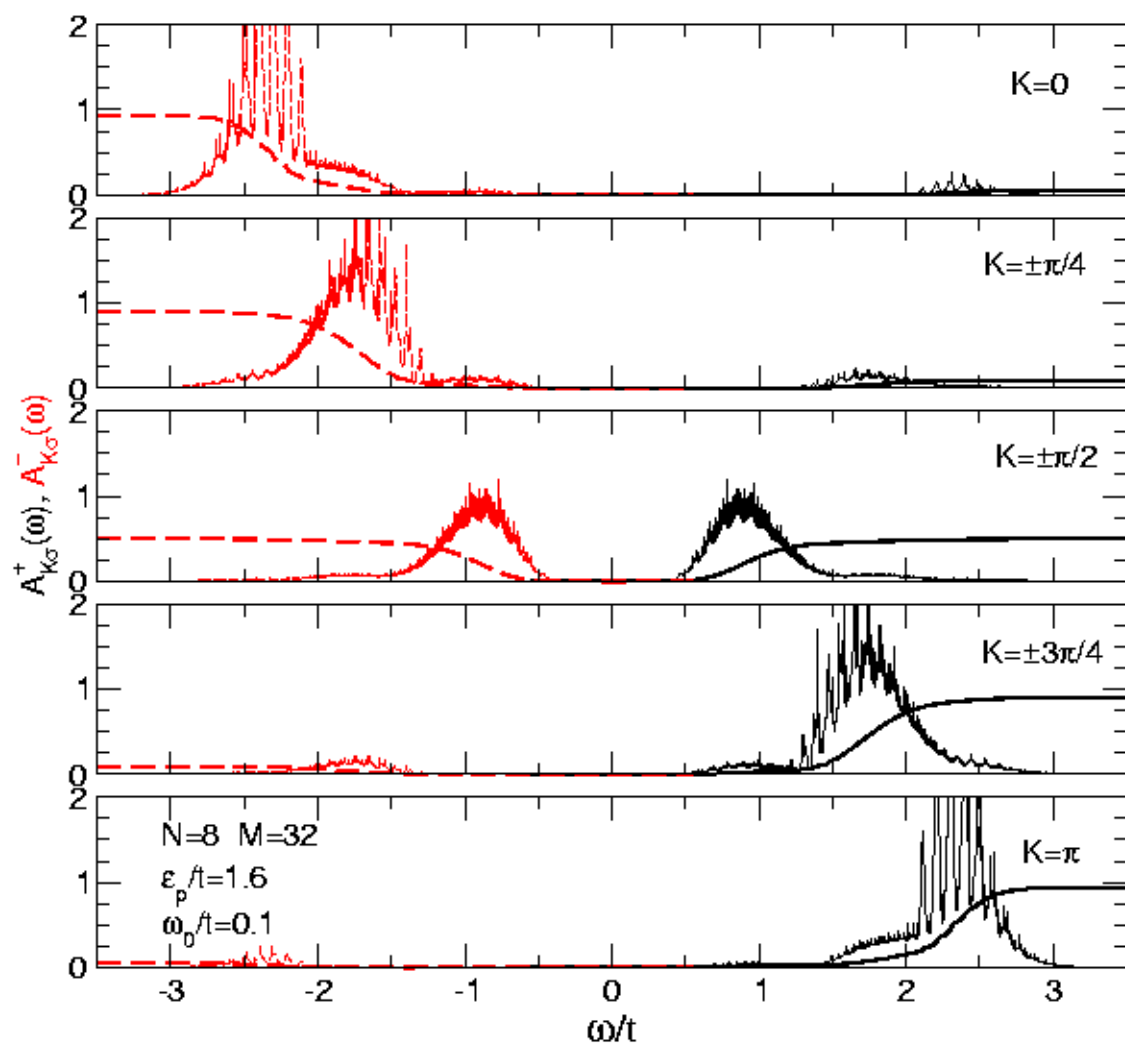


Fig. 4

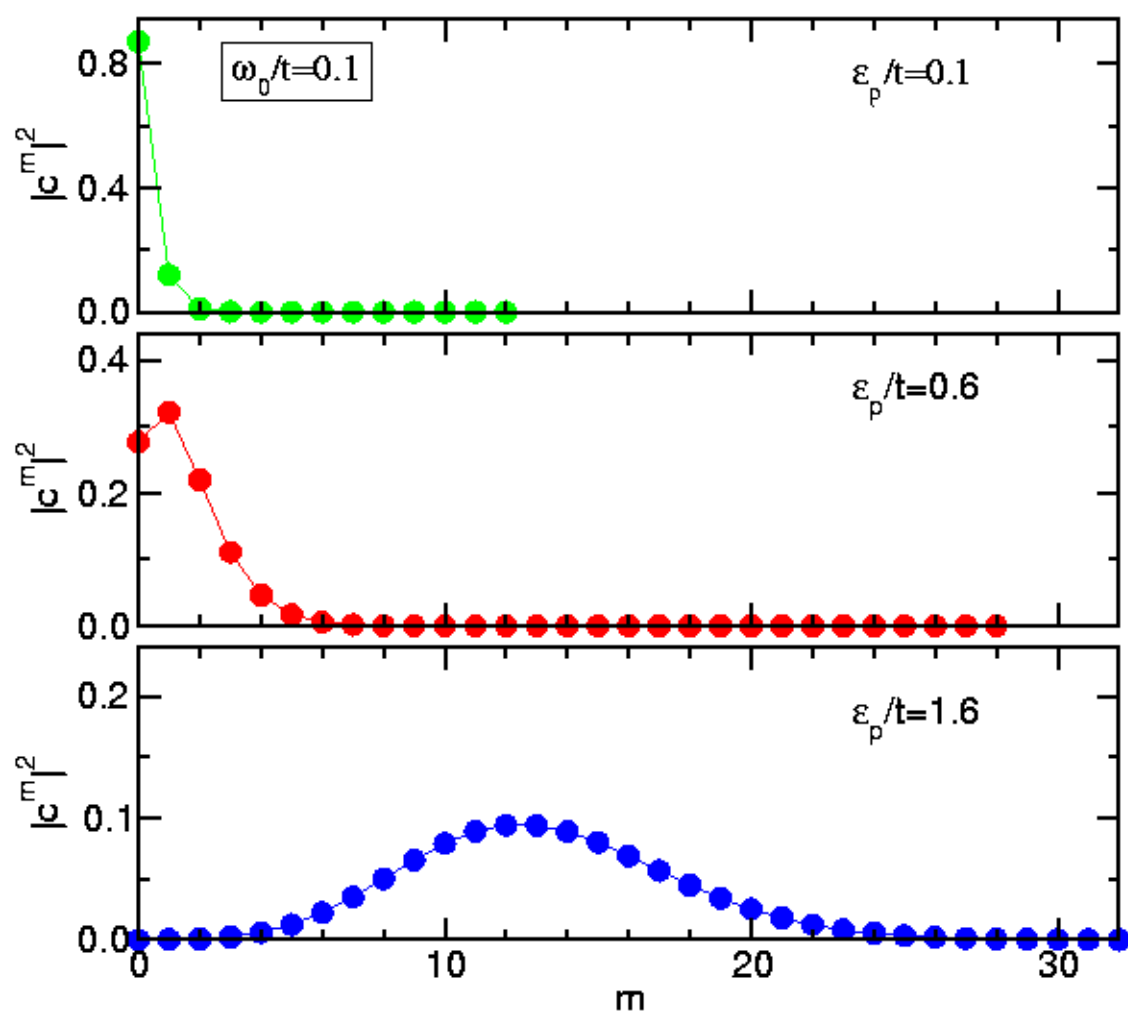


Fig. 5

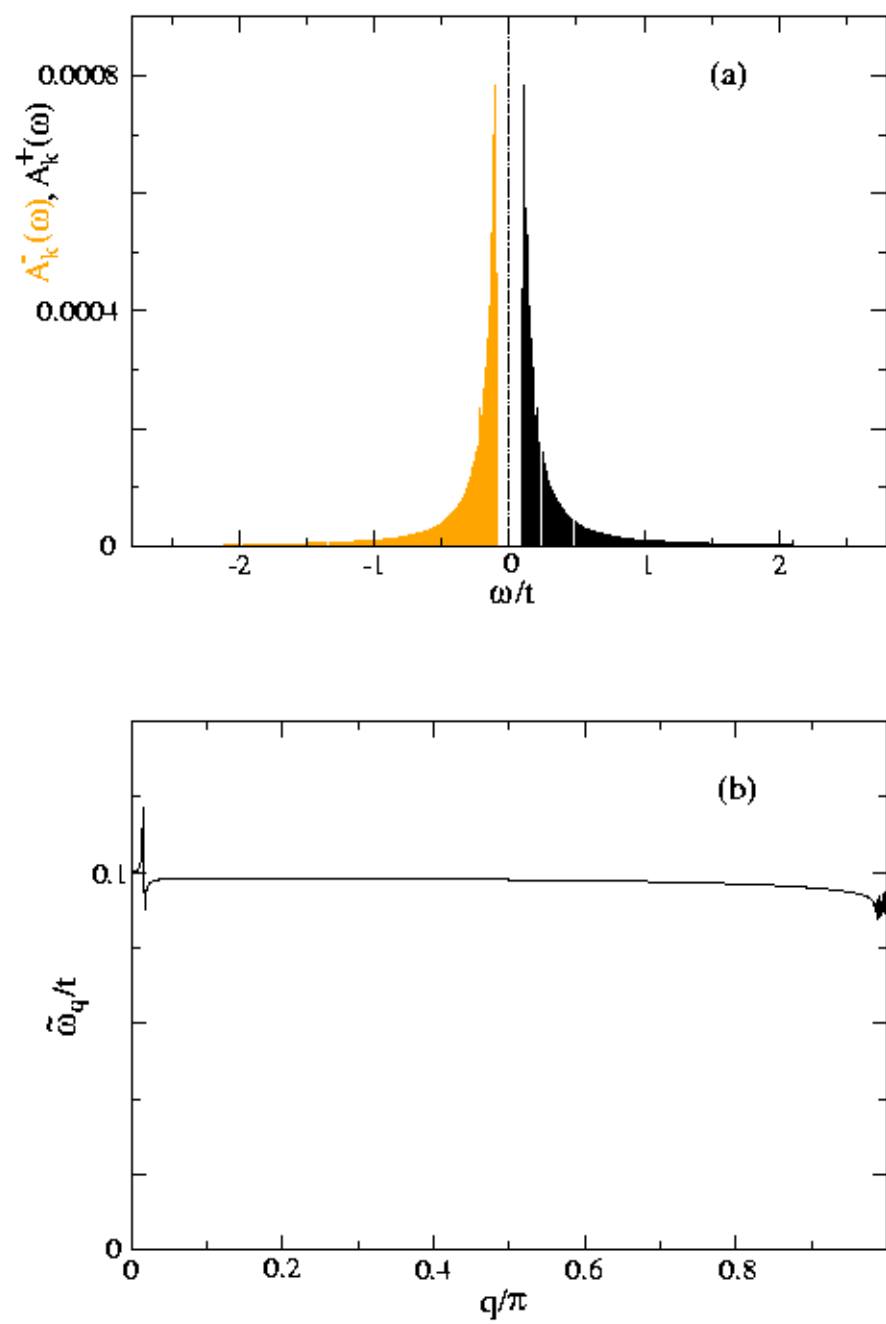


Fig. 6

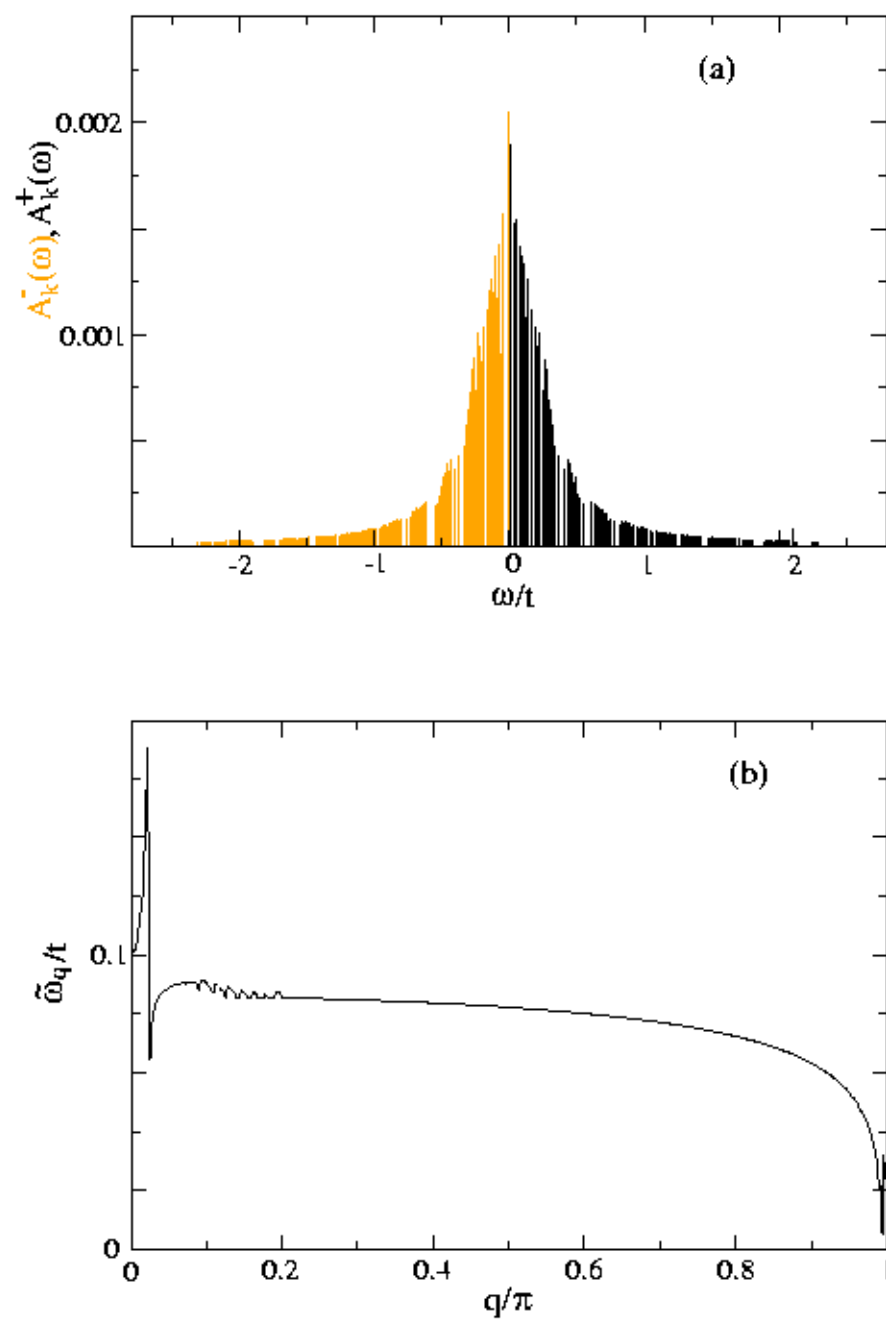


Fig. 7

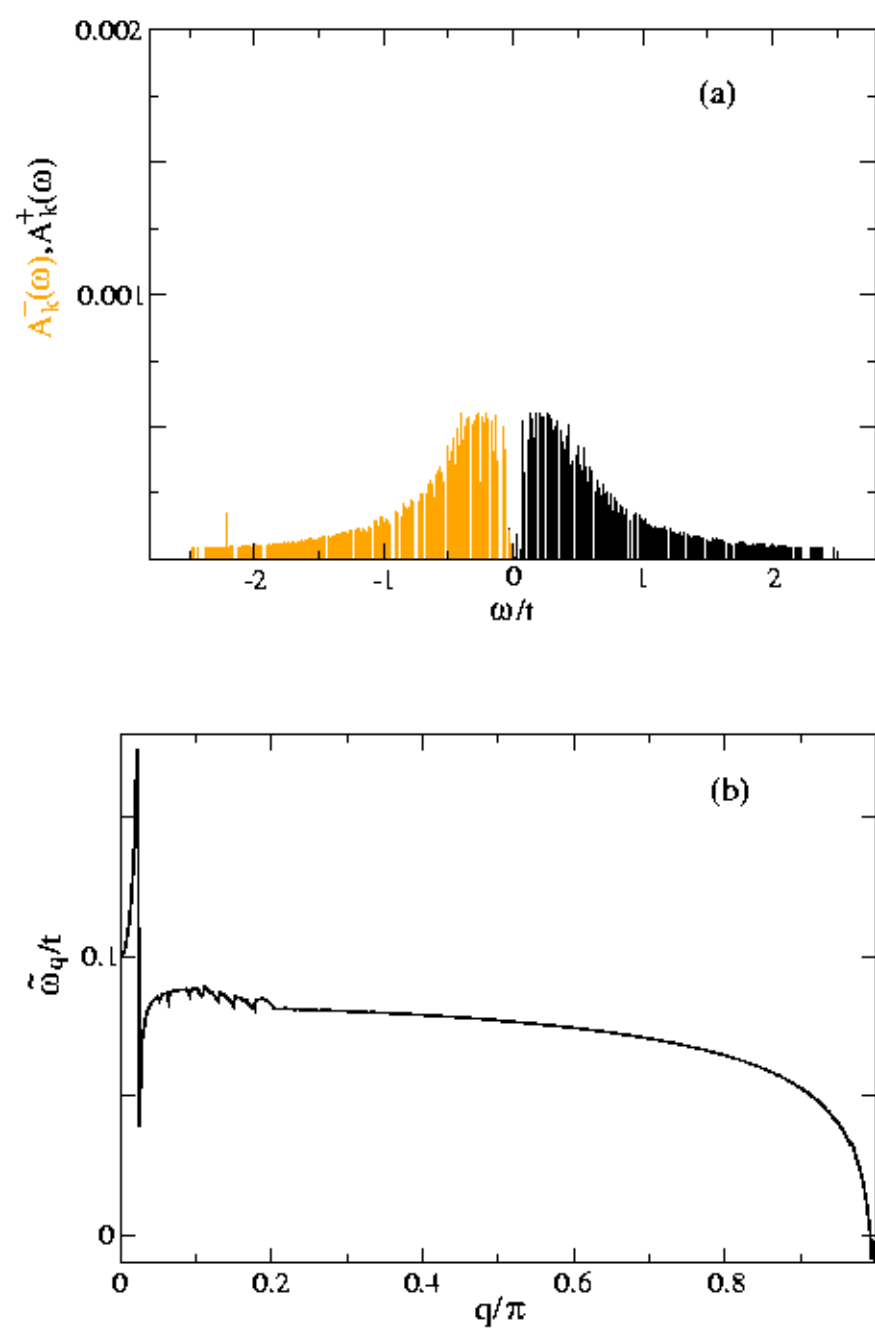


Fig. 8

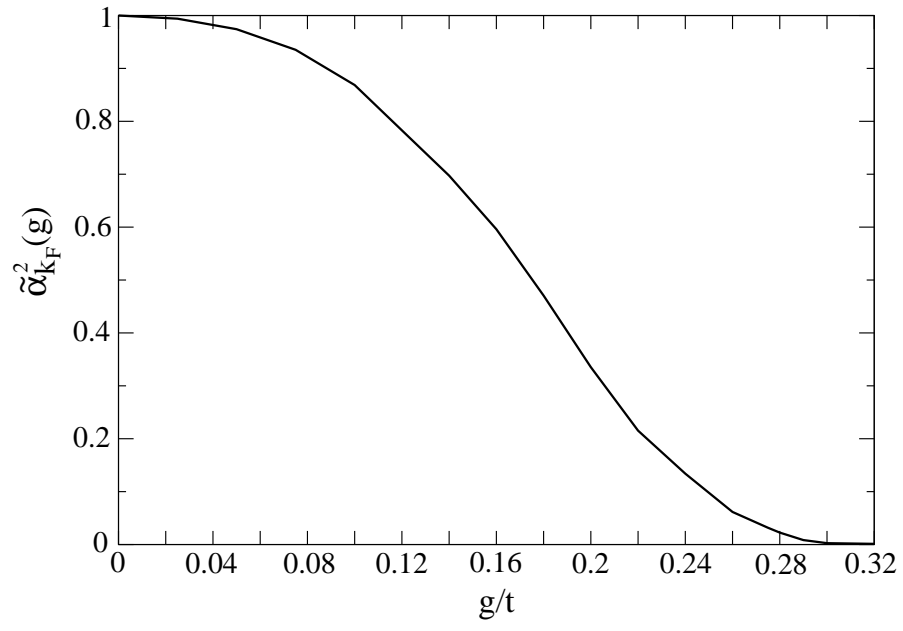


Fig. 9